

Performance Evaluation of Silicon-Carbide MOSFET in Three-Phase High-Power-Factor Rectifier

Yungtaek Jang, David L. Dillman, and Milan M. Jovanović
Power Electronics Laboratory
Delta Products Corporation
P.O. Box 12173, 5101 Davis Drive
Research Triangle Park, NC 27709

Abstract — A high-voltage silicon-carbide (SiC) power MOSFET was evaluated on two high-power factor (HPF), three-phase resonant rectifiers; a non-isolated, 2-kW buck rectifier and an isolated, 3-kW two-switch forward rectifier. By replacing an IGBT switch with a SiC power MOSFET switch that has an equivalent current rating, the efficiency of both the non-isolated and isolated resonant rectifiers were significantly improved.

The non-isolated buck rectifier using SiC MOSFET switches could deliver approximately 80%-40% more power than the rectifier using equivalent IGBT switches. Moreover, the efficiency of the isolated two-switch forward rectifier, which was operating with full load and switching frequency of 67 kHz, was improved by approximately 2% when IGBT switches were replaced by SiC power MOSFET switches. The IGBT loss was approximately 4.5% of the total output power. The loss of the SiC MOSFET was only 2.5% of the total output power under the same operating condition. When the prototype circuit was modified to operate at twice the switching frequency, the rectifier using SiC MOSFET switches could deliver approximately 60% more power than the rectifier using equivalent IGBT switches.

I. INTRODUCTION

A few silicon-carbide (SiC) switching devices have been introduced in the power electronics area during the last several years. Some commercial power supplies that employ SiC diodes are already available on the market. Moreover, the performance of SiC power FETs have been reported in [1]-[3]. Recently, Cree, Inc. introduced SiC MOSFET engineering samples for power conversion applications. To evaluate the performance of the high-voltage SiC power MOSFET, two three-phase, HPF resonant rectifiers were utilized, which were originally designed to employ IGBTs; a 2-kW non-isolated buck rectifier, and a 3-kW isolated two switch forward rectifier.

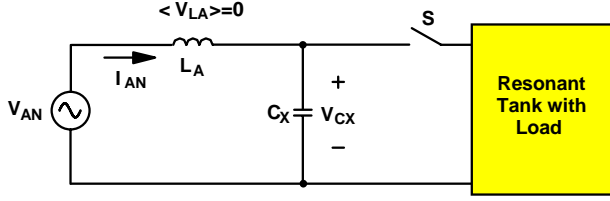
A non-isolated three-phase HPF topology employing a single switch was considered a good candidate since the overall performance of the rectifier depends significantly on the switch performance. In the past, several non-isolated

three-phase single-switch HPF rectifiers were introduced [4]-[11]. Generally, these single-switch circuits either employed a discontinuous-current-mode (DCM) pulse-width-modulation (PWM) boost rectifier topology [4]-[8] or resonant rectifier topologies [9]-[11]. To compare the performance between IGBTs and SiC MOSFETs, the three-phase HPF resonant buck rectifier introduced in [10] and [11] was employed, mainly because its switch operates with zero-current switching (ZCS), which is the optimum switching strategy for the IGBT switch. Although the tested three-phase HPF resonant buck rectifier exhibits many advantages such as HPF, soft-switching, and continuous input and output currents, the voltage stress on the switch device is approximately twice the peak input voltage, which makes using a conventional MOSFET challenging. As a result, IGBT switches are generally used for this rectifier topology. The problem faced by using the IGBT switch is that its conduction loss and switching loss greatly limit the rectifier efficiency at high frequency operation.

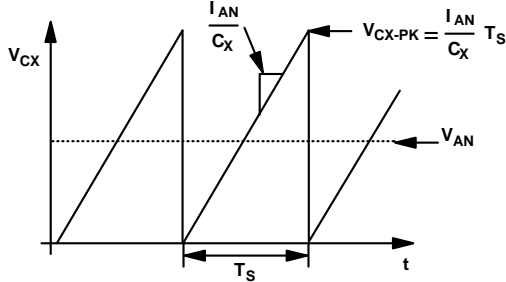
Recently, an isolated HPF ZCS two-switch forward resonant rectifier has been introduced in [12], which employs only two active switches compared to a conventional three-phase six-switch rectifier followed by an isolated dc-dc converter, which employs more than eight switches to achieve HPF and galvanic isolation between the input and output [13], [14]. Because of ZCS and the significant dependence of overall rectifier performance on switch performances, the isolated HPF ZCS two-switch forward resonant rectifier was also considered a good candidate.

In this paper, an evaluation comparing the IGBT and the SiC MOSFET was performed on a 2-kW HPF ZCS resonant buck rectifier operating from a three-phase input voltage of 220 V_{L-L}. Generally, the prototype circuit employing the IGBT switch could not deliver full power because of its switch's thermal instability while the circuit employing the SiC MOSFET switch delivered full load.

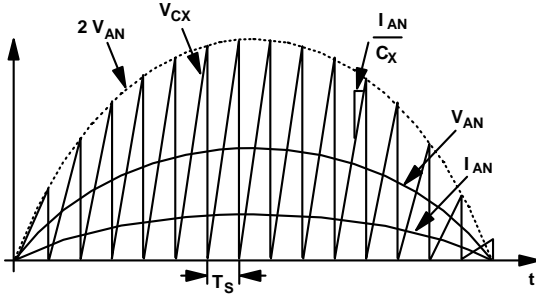
An isolated 3-kW HPF ZCS two-switch resonant rectifier operating from a three-phase 220 V_{L-L} input voltage was also



(a)



(b)



(c)

Fig. 1. (a) Single-phase DVM input circuit, (b) enlarged voltage waveform of capacitor C_X during one switching period, and (c) voltage waveform of capacitor C_X together with the input current and voltage waveforms during a half line cycle.

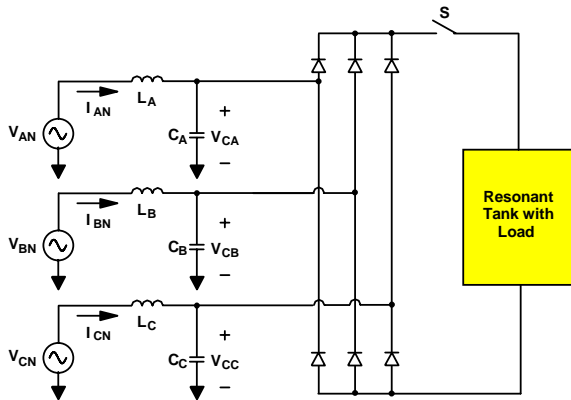


Fig. 2. Three-phase discontinuous-voltage-mode input circuit.

load by approximately 2%. When the prototype circuit was modified to operate at twice the switching frequency, the maximum output power of the rectifier using IGBT switches was limited to 1.8 kW by the thermal stress. However, the rectifier employing SiC power MOSFET switches delivered 60% more power than the rectifier employing IGBT switches when switches were within the allowable switch temperature. Therefore, by using SiC power MOSFETs instead of IGBTs, the maximum output power deliverable by the tested prototype circuit was significantly increased without thermal run-away of the switches.

II. REVIEW OF A THREE-PHASE HPF SINGLE-SWITCH RESONANT RECTIFIER

A. Discontinuous-Voltage-Mode Resonant Input

Figure 1 shows a single-phase discontinuous-voltage-mode (DVM) resonant input circuit and its voltage and current waveforms. If the stored energy in capacitor C_X immediately discharge through the resonant tank by turning on switch S , the voltage of capacitor C_X becomes discontinuous. Soon after switch S is turned off, input current I_{AN} flowing through input inductor L_A and starts charging capacitor C_X . Since input current I_{AN} is nearly constant during switching period T_S , and because input inductor L_A is a large filter inductor, the voltage of capacitor C_X increases linearly and proportionally to input current I_{AN} as shown in Fig. 1(b). The relationship between input current I_{AN} and input voltage V_{AN} is

$$V_{AN} = \frac{T_S}{2C_X} \times I_{AN}, \quad (1)$$

where T_S is the switching period of switch S . As shown in Fig. 1(c) and Eq. (1), if switching period T_S is nearly constant during the line cycle, input current I_{AN} becomes proportional to input voltage V_{AN} . As a result, the input of the DVM circuit behaves like a resistive impedance and achieves a high power factor.

Figure 2 shows a three-phase input circuit which has three input inductors L_A - L_C and three capacitors C_A - C_C . When switch S is turned off, the DVM circuit of each phase independently charges each capacitor. Moreover, when switch S is turned on, all the capacitors are immediately discharged. As a result, each phase circuit operates independently like the circuit shown in Fig. 1. Since the waveforms of input currents I_{AN} - I_{CN} follow their related input phase voltages, the rectifier achieves three-phase power-factor correction. It should be noted that input currents I_{AN} - I_{CN} include a harmonic component if the discharge of capacitors C_A - C_C is not linear. A linear discharge results in a low total-harmonic distortion (THD) and high power factor (PF). To achieve complete discharge of capacitors C_A - C_C in a short period of time, a resonant-type buck or buck-boost converter can be used.

evaluated. The SiC MOSFET switches improved the efficiency of the isolated two-switch forward rectifier at full

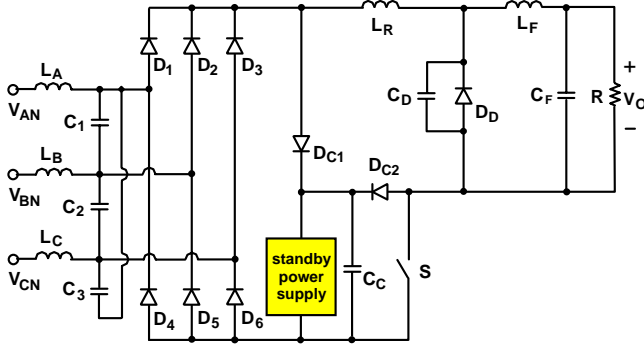


Fig. 3. Three-phase non-isolated resonant HPF buck rectifier.

B. 3-Phase HPF Resonant ZCS Buck Rectifier

A single-switch three-phase HPF resonant ZCS buck rectifier which operates in DVM is shown in Fig. 3. The major features of this rectifier are that both input and output currents are continuous and that a high power factor and low-harmonic rectification are achieved naturally. In addition, all semiconductor devices in this rectifier operate under soft-switching conditions. Specifically, the switch operates with zero-current turn-off, whereas the diodes operate with zero-voltage turn-on. Because of the ZCS of the switch, this circuit is suitable for the implementation of an IGBT. As shown in Fig. 3, the input side consists of input filter inductors L_A - L_C , input side capacitors C_1 - C_3 , input rectifiers D_1 - D_6 , and switch S . It should be noted that the switch voltages are clamped by clamp diodes D_{C1} and D_{C2} and clamp capacitor C_C . The voltage across clamp capacitor C_C is utilized as a dc source for the housekeeping power supply. The circuit also has resonant inductor L_R , output-side resonant capacitor C_D , output rectifier D_D , and output filter L_F with C_F connected across load R . In the circuit shown in Fig. 3, Y-connected input side capacitors C_A - C_C in Fig. 2 are converted to Δ -connected capacitors C_1 - C_3 , which is more desirable in power supply applications since they can be connected to both three-phase three-wire systems and three-phase four-wire systems. When switch S is turned on, the stored energy in C_1 - C_3 is quickly moved to resonant capacitor C_D through resonant inductor L_R . The discharging time is equal to one half resonant period T_O , which is approximately

$$T_O = 2\pi \sqrt{L_R \left(\frac{2CC_D}{2C + C_D} \right)}, \quad (2)$$

where $C=C_1=C_2=C_3$. Because the maximum effective capacitance of the Δ -connected capacitors that delivers the stored charge to the dc side of the bridge diodes is $2 \times C$, which happens when the two input phase voltages are equal, output resonant capacitor C_D is designed to be $2 \times C$. This is the best optimization because all of the charge in input resonant capacitors C_1 - C_3 can be moved to output resonant

capacitor C_D without having an unnecessarily big output resonant capacitor. By replacing C_D , Eq. (2) is simplified as

$$T_O = 2\pi \sqrt{L_R C}. \quad (3)$$

If resonant period T_O is designed to be relatively shorter than switching period T_S , the rectifier input current will have very small harmonic distortions. The detailed design procedure can be found in [10] and [11].

C. Three-Phase Isolated HPF Resonant ZCS Two-Switch Forward Rectifier

A three-phase six-switch rectifier followed by an isolated dc-dc converter is typically used in three-phase applications that require HPF and galvanic isolation between input and output. The rectifier circuit shown in Fig. 4 can achieve the same goal using only two switches. For cost sensitive applications, fewer switches and a simpler control circuit make this rectifier circuit very attractive. The circuit diagram of the isolated, HPF, resonant, ZCS, two-switch forward rectifier is shown in Fig. 4. The primary side consists of input filter inductors L_A - L_C , input side resonant capacitors C_1 - C_3 , input rectifiers D_1 - D_6 , switches S_1 and S_2 , and the primary winding of transformer TR . It should be noted that switch voltages are clamped by clamp diodes D_{C1} - D_{C3} and clamp capacitor C_C . The voltage across clamp capacitor C_C is utilized as both the transformer reset voltage and a dc source for the housekeeping power supply. The output side of the circuit consists of the secondary winding of transformer TR , resonant inductor L_R , secondary-side resonant capacitor C_D , forward diode D_F , output rectifier D_D , and output filter L_F with C_F connected across load R . The input capacitors of the rectifier shown in Fig. 4 are also configured as Δ -connection. It should be noted that resonant inductor L_R can be located in series with the primary winding or the secondary winding of transformer TR . Since resonant inductor L_R is in series with transformer TR , all of the leakage inductance of transformer TR becomes a part of the resonant inductor. When switches S_1 and S_2 are turned on, the stored energy in C_1 - C_3 is quickly moved to secondary-side resonant capacitor C_D through transformer TR and resonant inductor L_R . The discharging

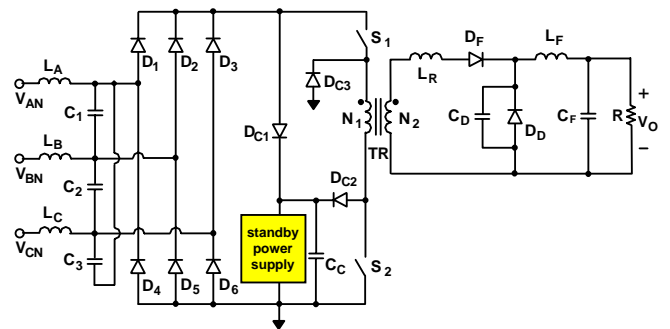


Fig. 4. Three-phase isolated resonant HPF two-switch forward rectifier.

time is approximately equal to one half of resonant period T_O , which is approximately

$$T_O = 2\pi\sqrt{L_R\left(\frac{2CC_D}{2C + n^2C_D}\right)}, \quad (4)$$

where $C=C_1=C_2=C_3$ and the turns ratio of transformer TR is $n=N_2/N_1$. If output resonant capacitor C_D is designed to be twice the value of capacitor C , Eq. (4) can be simplified as

$$T_O = 2\pi\sqrt{\frac{L_R}{n^2}C}. \quad (5)$$

For an optimal design, resonant period T_O to be relatively shorter than switching period T_S to achieve a low THD.

III. EXPERIMENTAL RESULTS

A. Specifications

Input:

- Three-phase, three-wire system, line-to-line voltage V_{IN} :
220 V_(L-L,RMS) ± 10%
- Line frequency f_L : 47 - 63 Hz
- THD: < 5%
- Power factor: > 0.98

Output:

- Voltage V_O :
 - 200 V_{DC}: non-isolated buck type rectifier
 - 400 V_{DC}: isolated two-switch forward rectifier
- Maximum output power P_O
 - 2 kW: non-isolated buck type rectifier
 - 3 kW: isolated two-switch forward rectifier
- Ripple voltage: < 12.5 V_{PEAK-PEAK} (300/360 Hz)

Cooling:

- Force convection

B. 2-kW HPF Resonant ZCS Buck Rectifier

A non-isolated HPF buck rectifier shown in Fig. 3 was built to deliver 2-kW of output power from a three-phase 220 V_{L-L} ± 10% input. Because the input line-to-line voltage is 220 V, effective input voltage $V_{NOM} = \frac{3}{2} \times V_{AN-PEAK} =$

$$\frac{3}{2} \times \frac{220\sqrt{2}}{\sqrt{3}} = 269.4 \text{ V.}$$

Since the employed converter topology is a buck-type rectifier, output voltage V_O is designed to be 200 V to maintain the regulation during an unexpected input-voltage transient. Because the desired maximum switching frequency is approximately 80 kHz, resonant frequency f_O was designed to be 130 kHz to have a ratio between switching period T_S and the reset period, which is one half of resonant period T_O , of more than three.

Three IGBTs and a SiC MOSFET were evaluated.

- Fairchild, FGL40N120AND, $V_{CES} = 1200 \text{ V}$, $I_{C100} = 40 \text{ A}$, TO-264, IGBT
- Fairchild, FGA25N120ANTD, $V_{CES} = 1200 \text{ V}$, $I_{C100} = 25 \text{ A}$, TO-3P, IGBT
- Fairchild, HGTG18N120BN, $V_{CES} = 1200 \text{ V}$, $I_{C110} = 26 \text{ A}$, TO-247, IGBT
- Cree, SiC MOSFET, $V_{DS} = 1200 \text{ V}$, $I_{D150} = 10 \text{ A}$, $R_{DS} = 100 \text{ m}\Omega$, TO-247,

To match the required current rating, two SiC MOSFETs were connected in parallel for switch S. Because the SiC MOSFET switches have a negative thermal feedback characteristic, the paralleled SiC MOSFETs evenly share the switch current.

High voltage diodes from Fairchild (FFAF10U170S, $V_{RRM} = 1700 \text{ V}$, $I_{FAVM} = 10 \text{ A}$) were employed as input bridge diodes D_1 - D_6 and output diode D_D . High voltage polypropylene capacitors with values of 68 nF (CDE, 940C20S68K, 2kV, 6.9 A_{RMS}) were used for input-side resonant capacitors C_1 - C_3 . Two polypropylene capacitors with values of 68 nF were connected in parallel and used as output-side resonant capacitor C_D . The total values of the input- and output-side resonant capacitors were 68 nF and 136 nF, respectively.

The desired inductance for input filter inductors L_A , L_B , and L_C was 300 μH for each phase. Two high-flux toroidal cores (Arnold, HF488075-2) were used in parallel to reduce flux density and the number of winding turns. A magnet wire (45 turns, AWG# 13) was used as the inductor winding.

The inductance of resonant inductor L_R was 22 μH to obtain the desired resonant frequency of 130 kHz. A set of ferrite EE cores (ETD54/27/19-87, air gap=6 mm) was used for resonant inductor L_R . Litz wire (435 strands, AWG# 40, 10 turns) was used to reduce the proximity effect of the winding.

The inductance of output filter inductor L_F was 900 μH . A set of ferrite EE cores (E65/32/27-3C94, air gap=40 mils) was used for output filter inductor L_F . A solid magnet wire (50 turns, AWG# 12) was used because the proximity effect in the output filter inductor was negligible.

C. 3-kW, HPF, Resonant, ZCS, Two-Switch Forward Rectifier

An isolated HPF two-switch forward rectifier shown in Fig. 4 was built to deliver 3-kW of output power from a three-phase 220 V_{L-L} ± 10% input. Two IGBTs (FGL40N120AND, FGA25N120ANTD) and a SiC MOSFET (Cree, 10 A, 1200 V) were evaluated on this prototype circuit. To match the required current rating, two SiC MOSFETs were connected in parallel for both switches S_1 and S_2 .

High voltage diodes from Fairchild (FFAF10U170S) were employed as secondary side forward diode D_F , input bridge diodes D_1 - D_6 , and output diode D_D . High voltage

polypropylene capacitors with values of 100 nF (CDE, 940C20P1K, 2kV, 8.3 A_{RMS}) and 10 nF (CDE, 940C30S1K, 3kV, 2 A_{RMS}) were used in parallel for input-side resonant capacitors C₁-C₃. Two polypropylene capacitors with values of 47 nF (CDE, 940C20S47K, 2kV, 5.2 A_{RMS}) and 10 nF were connected in parallel and used for output-side resonant capacitor C_D. The total values of the input- and output-side resonant capacitors were 110 nF and 57 nF, respectively.

The desired inductance for input filter inductors L_A, L_B, and L_C was 300 μH for each phase. Two high-flux toroidal cores (Arnold, HF488075-2) were used in parallel for the input filter inductors. A magnet wire (45 turns, AWG# 13) was used as the inductor winding.

Two sets of EE cores (E80/38/20-3C94, air gap=1 mil) were used in parallel to construct isolation transformer TR. Two Litz wires (435 strands, AWG# 40, 22 turns) connected in parallel were used as the primary winding and a Litz wire (435 strands, AWG# 40, 44 turns) was used as a secondary winding of the transformer. It should be noted that turns ratio n of transformer TR is 2, which makes the rectifier deliver a 400 V output voltage.

The inductance of resonant inductor L_R had to be 80 μH to obtain the desired resonant frequency of 108 kHz. A set of ferrite EE cores (ETD44/21-3F3, air gap=6 mm) was used for resonant inductor L_R. Litz wire (435 strands, AWG# 40, 45 turns) was used to reduce the proximity effect of the winding. It should be noted that the performance of the prototype circuit was measured after the resonant frequency was modified to be two times higher than the original resonant frequency. To increase the resonant frequency, all the values of resonant capacitors C₁-C₃ and C_D and resonant inductor L_R were reduced to one half of each original value.

Finally, the inductance of output filter inductor L_F was 900 μH. A set of ferrite EE cores (E65/32/27-3C94, air gap=40 mils) was used. A solid magnet wire (50 turns, AWG# 12) was used.

D. Measured Results of 2-kW HPF Buck Rectifier

A non-isolated HPF buck rectifier described in Section III-B employing a SiC MOSFET was tested to measure the waveforms at the full load. Figure 5 shows the measured waveforms of the input line currents delivering 2 kW from the three-phase line-to-line input voltage V_{IN} = 220 V. Results demonstrated THD of less than 6% at full output power. Figures 6(a)-6(b) show the measured waveforms of key components. All the measured waveforms in Fig. 6 have the same time scale and aligned to the equal trigger moment. Figure 6(a) shows the measured voltage waveforms of input resonant capacitors C₁-C₃. The input capacitor voltages are discontinuous. The switching frequency at full load is approximately 83 kHz, the ratio between switching period T_S and the reset period that is one half of resonant period T_O is approximately three times. It should be noted that the input current THD becomes smaller when the output power

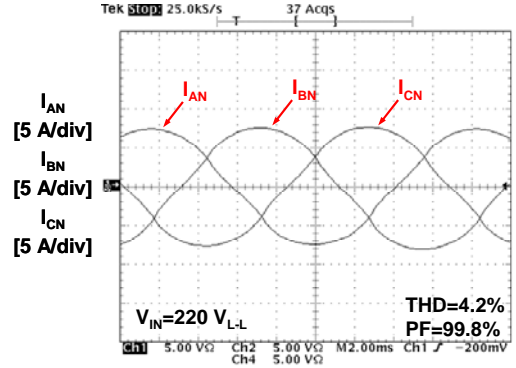


Fig. 5. Measured three-phase input current waveforms of the experimental HPF resonant buck converter prototype at P_O=2 kW, f_o=130 kHz, and V_{IN}=220 V_{L-L}. Time base: 2 ms/div.

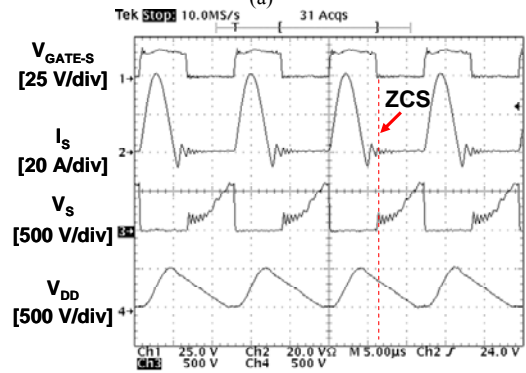
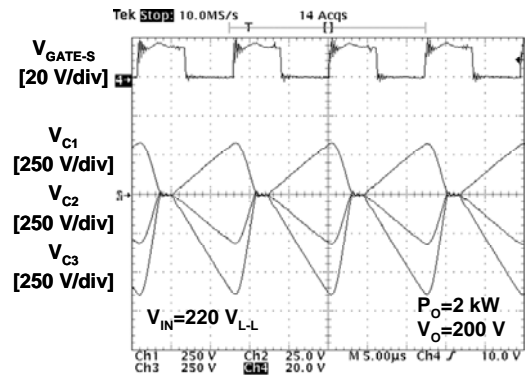


Fig. 6. Measured waveforms of the experimental HPF buck converter prototype at V_{IN}=220 V_{L-L}, V_O=200 V_{DC}, f_o=130 kHz, and P_O=2 kW. Time base: 5 μs/div.

becomes lower since the switching frequency decreases monotonically when the load decreases, *i.e.*, the ratio between switching period T_S and the reset period increases. Figure 6(b) shows the measured current and drain-to-source voltage waveforms of switch S. As shown in the figure, switch S turns off when switch current I_S reaches zero.

Figure 7 shows measured efficiencies and temperatures of the prototype circuit with three different types of IGBTs (FGL40N120AND, FGA25N120ANTD, HGTG18N120BN)

and a SiC MOSFET (Cree, 10 A, 1200 V). The performance of the test circuit employing each IGBT switch was measured and recorded. The same prototype circuit except for using SiC MOSFET was used to measure the performance. As can be seen from Fig. 7(a), the prototype circuit employing a SiC MOSFET switch improves the conversion efficiency in the entire measured power range (600W to 2 kW). Nevertheless, the efficiency improvement is more pronounced at higher power levels where conduction loss and switching losses are greater. Specifically, the prototype circuit employing FGA25N120ANTD and HGTG18N120BN cannot deliver more than approximately 1.8 kW and 1.2 kW, respectively. The prototype circuit employing FGL40N120AND was able to deliver up to 2 kW. As shown in Fig. 7(b), the temperatures of the IGBT switches become unstable at each maximum load. The prototype circuit employing the SiC MOSFET were able to deliver full power. Moreover, the temperatures of the two parallel SiC MOSFET switches were 54 °C and 45 °C at full load, respectively.

Figure 7(b) shows the measured temperatures of the

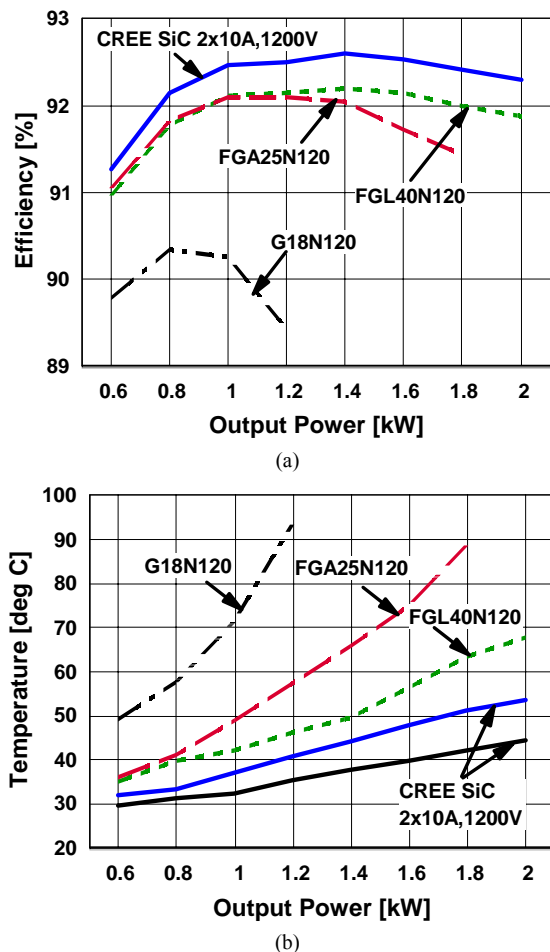


Fig. 7. Measured efficiency (a) and temperature (b) of the experimental three-phase HPF buck converter with IGBTs (dashed line) and SiC MOSFET (solid line) at $V_{IN}=220 V_{L-L}$, $f_0=130$ kHz, and $V_0=200$ V as functions representing output power.

experimental converter with SiC MOSFET (solid line) and IGBT (dashed lines) functions of the output power. The ambient temperature was approximately 26°C during the measurement. As can be seen from Fig. 7(b), at the same power levels, the temperatures of the SiC MOSFET switch are significantly lower than those in the implementation with the IGBTs. As indicated in Fig. 7(b), at 2 kW output power, which is the maximum output power the largest IGBT can deliver, the case temperature of the SiC MOSFET in the prototype circuit is 54 °C, whereas the corresponding temperature of the IGBT (FGL40N120AND) in the prototype circuit is 70 °C, which is significantly higher than that of the SiC MOSFET.

E. Measured Results of 3-kW HPF Two-Switch Forward Rectifier

The isolated HPF two-switch forward rectifier described in Section III-C was tested. Figure 8 shows the measured waveforms of the input line currents delivering 3 kW from the three-phase line-to-line input voltage $V_{IN} = 220$ V. Results show THD of less than 5% at full output power. Figures 9(a)-9(b) show the measured waveforms of key components. All the measured waveforms in Fig. 9 have the same time scale and aligned to the equal trigger moment. Figure 9(a) shows the measured gate-to-source voltage of switch S_2 and the measured voltage waveforms of input resonant capacitors C_1-C_3 . The input capacitor voltages are discontinuous. When the switching frequency at full load is approximately 67 kHz, the ratio between switching period T_S and the reset period, which is one half of resonant period T_O , is approximately 3.2. Figure 9(b) shows the measured current and drain-to-source voltage waveforms of switch S_2 . As indicated in Fig. 9(b), switches S_1 and S_2 are turned off with ZCS.

The efficiencies and temperatures of the prototype circuit with two different types of IGBTs (FGL40N120AND, FGA25N120ANTD) and a SiC MOSFET (Cree, 10 A, 1200 V) were measured as shown in Fig. 10. Since the performance of HGTG18N120BN was not better than those

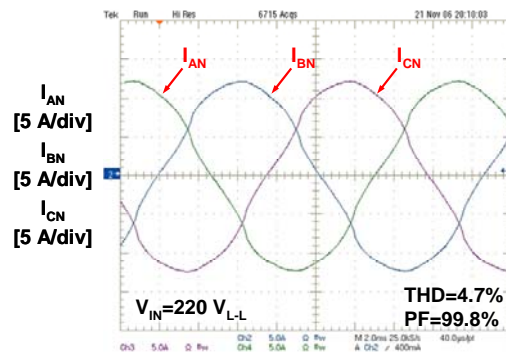


Fig. 8. Measured three-phase input current waveforms of the experimental HPF resonant two-switch forward converter prototype at $P_0=3$ kW, $f_0=108$ kHz, and $V_{IN}=220 V_{L-L}$. Time base: 2 ms/div.

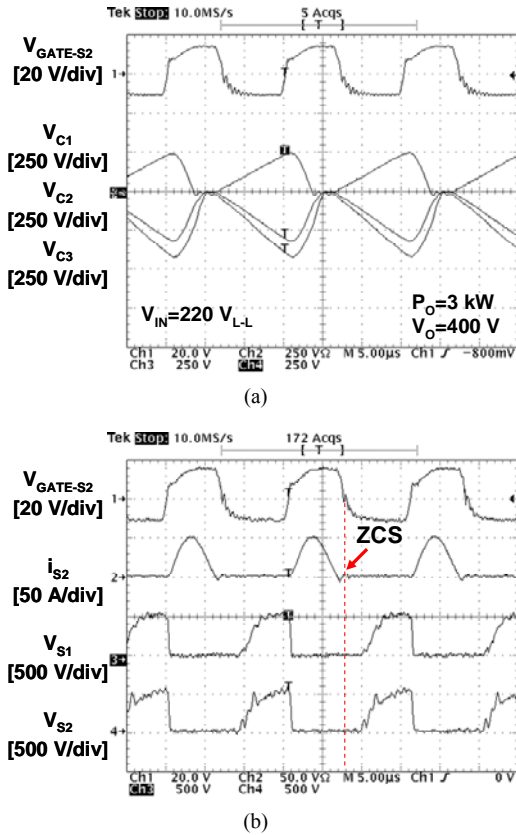


Fig. 9. Measured waveforms of the experimental HPF two-switch forward converter prototype at $V_{IN}=220 V_{L-L}$, $V_O=400 V_{DC}$, $f_0=108 \text{ kHz}$, and $P_O=3 \text{ kW}$. Time base: $5 \mu\text{s}/\text{div}$.

of other types of IGBTs used in the previous evaluation with the HPF buck rectifier prototype circuit, the HGTG18N120BN was excluded during this evaluation. As can be seen from Fig. 10(a), the prototype circuit employing a SiC MOSFET switch improves the conversion efficiency in the entire measured power range (300 W to 3 kW). Nevertheless, the efficiency improvement is more pronounced at higher power levels where conduction loss and switching losses are greater. The efficiency improvement was approximately 2%, which translates to 20% reduction of loss.

Figure 10(b) shows the measured temperatures of the experimental converter with SiC MOSFET (solid line) and IGBT (dashed lines) functions of the output power. The ambient temperature was approximately 26°C during the measurement. As can be seen from Fig. 10(b), when at the same power levels, the temperatures of the SiC MOSFET switch were significantly lower than those of the implementation with the IGBTs. As indicated in Fig. 10(b), at full power the case temperature of the SiC MOSFET in the prototype circuit was 55°C , whereas the corresponding temperatures of the FGL40N120AND and FGA25N120ANTD in the prototype circuit were 80°C and 90°C , respectively, which are significantly higher than that of the SiC MOSFET.

To evaluate the performance of the switches at a higher switching frequency, resonant frequency f_0 of the prototype circuit was multiplied by two, *i.e.*, switching frequency f_0 was doubled to deliver the same output power. THD of the input current was less than 5% at 2.4 kW of output power.

The efficiencies and temperatures of the prototype circuits associated with the two different types of IGBTs (FGL40N120AND, FGA25N120ANTD) and the SiC MOSFET (Cree, 10 A, 1200 V) were measured as shown in Fig. 11. As can be seen from Fig. 11(a), the prototype circuit employing a SiC MOSFET switch can deliver full power while the prototype circuit employing FGL40N120AND and FGA25N120ANTD can only deliver 1.8 kW and 1.5 kW, respectively. Figure 11(b) shows the measured temperatures of the experimental converter with SiC MOSFET (solid line) and IGBT (dashed lines) functions of the output power. The ambient temperature was approximately 26°C during the measurement. As can be seen from Fig. 11(b), when at the same power levels, the temperatures of the SiC MOSFET switch are significantly lower than those of the

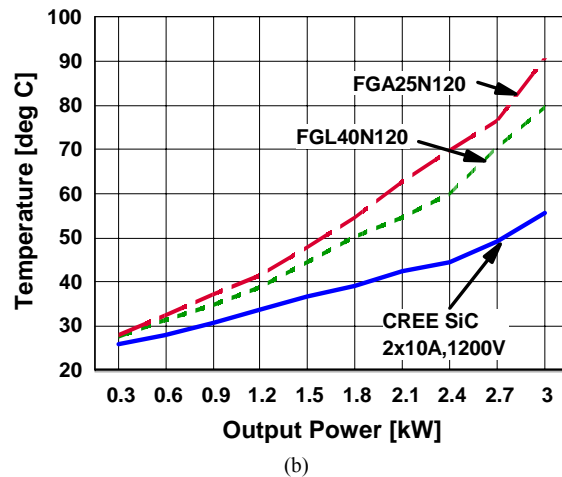
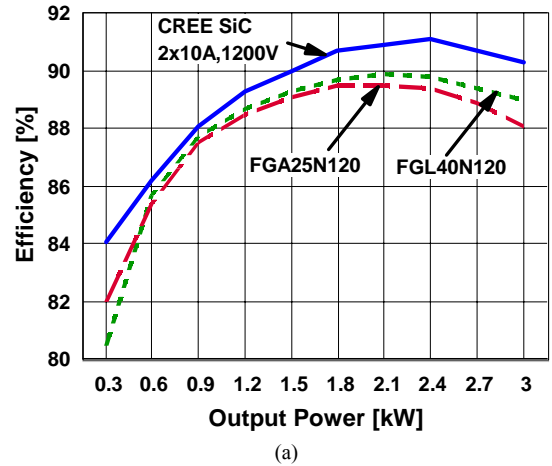


Fig. 10. Measured efficiency (a) and temperature (b) of the experimental three-phase HPF two-switch forward converter with IGBTs (dashed line) and SiC MOSFET (solid line) at $V_{IN}=220 V_{L-L}$, $f_0=108 \text{ kHz}$, and $V_O=400 \text{ V}$ as functions representing output power.

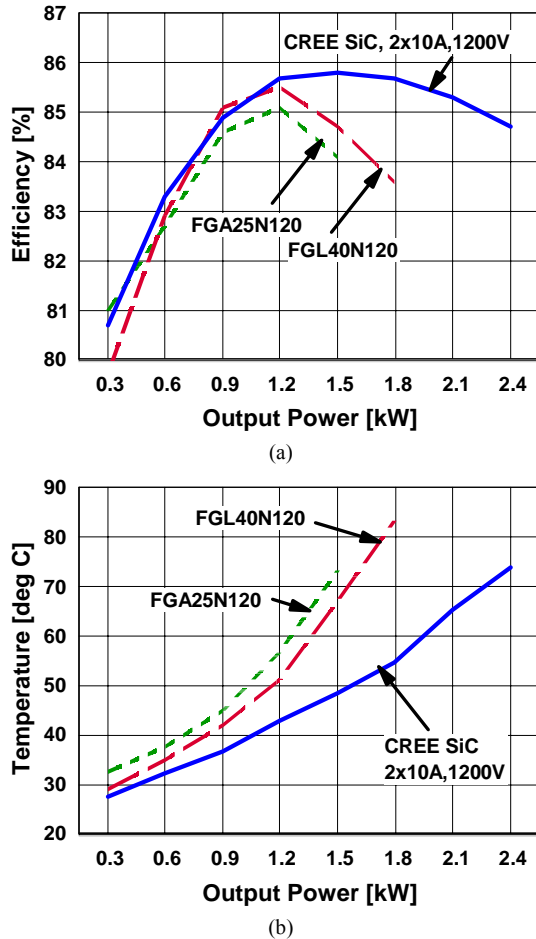


Fig. 11. Measured efficiency (a) and temperature (b) of the experimental three-phase HPF two-switch forward converter with IGBTs (dashed line) and SiC MOSFET (solid line) at $V_{IN}=220$ V_{L-L}, $f_0=216$ kHz, and $V_0=400$ V as functions representing output power.

implementation with the IGBTs.

IV. SUMMARY

The performance of a three-phase HPF non-isolated 2-kW buck resonant rectifier and an isolated 3-kW two-switch forward resonant rectifier that employ high-voltage SiC power MOSFETs or IGBTs have been evaluated. By replacing an IGBT switch with a SiC power MOSFET switch, the efficiency of the non-isolated 2-kW buck resonant rectifier significantly improved. Moreover, the efficiency of the isolated 3-kW two-switch forward rectifier was also improved by approximately 2% when IGBT switches were replaced by SiC power MOSFET switches. The IGBT loss was approximately 4.5% of the total output power. The loss of the SiC MOSFET was only 2.5% of the total output power under the same operating condition. When the prototype circuit was modified to operate at twice the switching frequency, the rectifier using SiC MOSFET

switches could deliver approximately 60% more power than the rectifier using equivalent IGBT switches.

ACKNOWLEDGEMENT

We would like to thank CREE, Inc. for supplying the product information and beta version SiC MOSFET samples.

REFERENCES

- [1] C. J. Cass, Y. Wang, R. Burgos, T. P. Chow, F. Wang, and D. Boroyevich, "Evaluation of SiC JFETs for a three-phase current-source rectifier with high switching frequency," *IEEE Applied Power Electronics Conf. (APEC) Record*, pp. 345 – 351, 2007.
- [2] T. Funaki, M. Matsushita, M. Sasagawa, T. Kimoto, and T. Hikiyama, "A study on SiC devices in synchronous rectification of dc-dc converter," *IEEE Applied Power Electronics Conf. (APEC) Record*, pp. 339 – 344, 2007.
- [3] M. L. Heldwein and J. W. Kolar, "A novel SiC J-FET gate drive circuit for sparse matrix converter application," *IEEE Applied Power Electronics Conf. (APEC) Record*, pp. 116 – 121, 2004.
- [4] L. Simonetti, J. Sebastian, and J. Uceda, "Single-Switch Three-Phase Power Factor Under Variable Switching Frequency and Discontinuous Input Current," *IEEE Power Electronics Specialists Conf. (PESC) Record*, pp. 657 - 662, 1993.
- [5] J. W. Kolar, H. Ertl, and F. C. Zach, "Space Vector-Based Analytical Analysis of the Input Current Distortion of A Three-Phase Discontinuous-Mode Boost Rectifier System," *IEEE Power Electronics Specialists Conf. (PESC) Record*, pp. 696 - 703, 1993.
- [6] Q. Huang and F. C. Lee, "Harmonic Reduction in A Single-Switch, Three-Phase Boost Rectifier with High Order Harmonic Injected PWM," *IEEE Power Electronics Specialists Conf. (PESC) Record*, pp. 1266 - 1271, 1996.
- [7] J. Sun, N. Frohliche, and H. Grotstollen, "Harmonic Reduction Techniques for Single-Switch Three-Phase Boost Rectifiers," *Conference Record of the 1996 IEEE Industry Applications Society Annual Meeting*, pp. 1225 - 1232, 1996.
- [8] Y. Jang and M. M. Jovanović, "A New Input-Voltage Feedforward Harmonic-Injection Technique with Nonlinear Gain Control for Single-Switch, Three-Phase DCM Boost Rectifier," *IEEE Transactions on Power Electronics, Vol. 15, no. 2*, pp. 268-277, March 2000.
- [9] E. H. Ismail and R. W. Erickson, "A single transistor three-phase resonant switch for high quality rectification," *IEEE Power Electronics Specialists Conf. (PESC) Record*, pp. 1341 – 1351, 1992.
- [10] Y. Jang and R. W. Erickson, "New single-switch three-phase high power factor rectifiers using multi-resonant zero current switching," *IEEE Applied Power Electronics Conf. (APEC) Record*, pp. 711 – 717, 1994.
- [11] Y. Jang, M. M. Jovanović, "Design Considerations and Performance Evaluation of a 6-kW, Single-Switch, Three-Phase, High-Power-Factor, Multi-Resonant, Zero-Current-Switching Buck Rectifier," *International Telecommunications Energy Conf. (INTELEC) Record*, pp. 715 - 722, 1997.
- [12] Y. Jang, D. L. Dillman, and M. M. Jovanović, "Three-Phase Isolated High-Power-Factor Rectifier Using Soft-Switched Two-Switch Forward Converter," *IEEE Applied Power Electronics Conf. (APEC) Record*, pp. 809 – 815, 2007.
- [13] A. R. Prasad, P. D. Ziogas and S. Manias, "An active power factor correction technique for three-phase diode rectifiers," *IEEE Power Electronics Specialists Conf. (PESC) Record*, pp. 58 – 66, 1989.
- [14] H. Mao, D. Boroyevich, A. Ravindra, and F. C. Lee, "Analysis and Design of High Frequency Three-phase Boost Rectifiers," *IEEE Applied Power Electronics Conf. (APEC) Record*, pp. 538 – 544, 1996.